Effect of Rotor bar Shape on the Performance of Three Phase Induction Motors with Broken Rotor Bars

Evelin Maloma, Mbika Muteba and Dan-Valentin Nicolae
University of Johannesburg, South Africa

Abstract- **A slight change in time phase shift between currents in adjacent rotor end ring segments directly affects the characteristics of the airgap torque in a squirrel cage induction machine (SCIM). On the other hand the rotor slot geometrical permeance has a strong impact on the rotor bar leakage inductance. This paper deals with effect of different rotor bar types (geometrical shapes) when a SCIM operates under healthy and broken rotor bars condition. The three phase squirrel cage induction machine is designed and modelled using two dimension (2D) finite Element Model (FEM). Static and dynamic analysis are performed in order to determine the target performance indexes such as transient torque, steady state torque, torque ripple, air-gap flux density, power factor and efficiency. The Finite Element Analysis (FEA) results evidence that the rotor bar shape can be optimized, such that the SCIM is yet to produce good performance when the phase shift between neighbouring bars e.m.f is changed due to rotor bar breakage.**

I. INTRODUCTION

SCIMs are the most popular induction machine types in industry today, the reasons behind their intensive use is their robust design, simple construction, low cost and ease maintenance [5, 10, 11, 28]. Despite the mentioned advantages, three phase SCIMs have this problem of rotor bar breakage [1, 2].

A better design of SCIMs in order to improve their performance taking into account the broken rotor bar fault which generally affects the performance of these machines will benefit industry. In literature [11, 12, 13] major focus has been working towards finding an optimal design of induction machine geometry with the aim of improving the performance. In [11, 12] a generic algorithm approach was used to achieve an optimal design of induction machine with the aim of reducing losses and therefore improving the power factor and efficiency of the machine.

Several literature studies have been published on improving induction machine performance through geometry re-design, with much focus on stator slot opening, stator and rotor bar shape and use of magnetic and non-magnetic wedges [3, 4, 6, 8, 9, 14]. No work was dedicated to re-designing the geometry of the induction machine (particularly the rotor bar shape) in view of enhancing the performance of SCIMs when rotor bars are broken.

The purpose of this paper is therefore to analyse the influence of different rotor bar shapes upon performance of the motor. Five available rotor bar shapes are used.

The model will be used to study the behaviour of the machine for various shapes of the rotor bars under both healthy and faulty conditions. In the case of broken rotor bars, all broken bars are adjacent. The rotor bar skin effect will be considered whereas skewing will not be taken into account. During induction motor start-up, the current migrates to the top of the bar (lowest impedance region) as a result of skin effect. The current migration results in temperature gradient as the top part of the bar heats-up faster than the lower part (lower impedance region). As the rotor accelerates, the current will be evenly distributed throughout the entire bar, this phenomenon is called skin effect. Skin effect in rotor bars is intentionally used in design of SCIMs in order to develop a high starting current and a lower stator current [26, 27].

According to literature [26], the skin effect will vary as the shape of rotor and rotor bars change. Changes in rotor bar shapes will result in different resistances at different depths of the rotor bar and this will yield increased or decreased electromagnetic torque. With the five different rotor bar shapes, the area of the upper body of the bars will differ resulting in different effective resistance and different starting torque. Both magneto-static and transient analysis of the machine model will be performed while comparing different performance parameters of the machine.

II. MACHINES RATINGS AND SPECIFICATIONS

This study is based on 36 stator slots and 33 rotor slots three phase, low voltage SCIM whose specification and ratings are shown in Fig. 1. , Table I and Table II below.

TABLE I
MOTOR RATING

Parameter	Value
Rated Output Power	5.5 kW
Number of Phases	3
Rated Voltage	400 V
Rated Current	11.59 A
Rated Speed	1360
Number of poles	4
Frequency	50Hz

In Table III, the dimensions of the rotor slot for the conventional machine (with rotor bar type 1) is presented. Four other available rotor bar types are presented in Fig. 2.

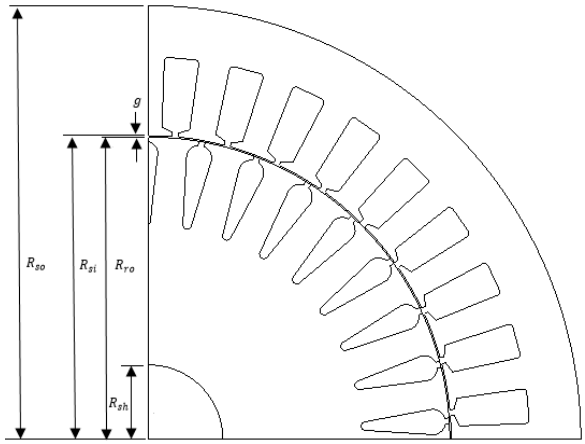

Fig. 1. Motor Specification

TABLE II
MOTOR SPECIFICATIONS

Parameter	Value (mm)
Stator Outer Radius _R_{so}	105
Stator Inner Radius _R_{si}	73.5
Rotor Outer Radius _R_{ro}	73.15
Airgap Length (g)	0.35
Shaft Radius _R_{sh}	18

TABLE III
ROTOR BAR TYPE 1 DIMENSIONS

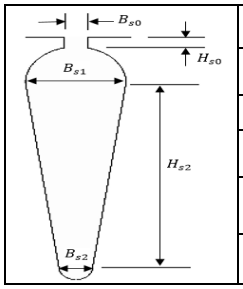

Parameter	Value (mm)
Slot opening height_Hs0	1
Slot body height _Hs2	16.38
Slot opening width_Bs0	1.5
Slot wedge maximum width_Bs1	6.16

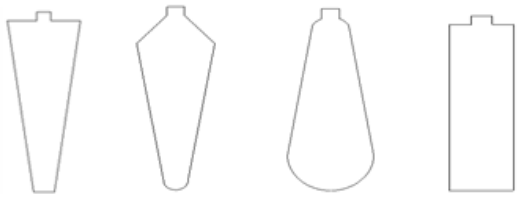

Fig. 2. Representation of different rotor bar shapes; (a) Type 2, (b) Type 3, (c) Type 4 and (d) Type 5.

III FAULTLESS ROTOR CAGE MODEL

The SCIM analyzed in this paper has no-integral number of rotor bars per pole. It is better to model the cage as having a number of identical magnetically coupled circuits [24]. The rotor cage equivalent circuit representing the impedance nature of the circuit $Z = (R + jX)$, with symmetric faultless rotor cage bars [22, 23] is depicted in Fig 3 (a), and its current phasor representation is shown in Fig 3(b). The rotor resistance and rotor inductance matrixes are well detailed in [24].

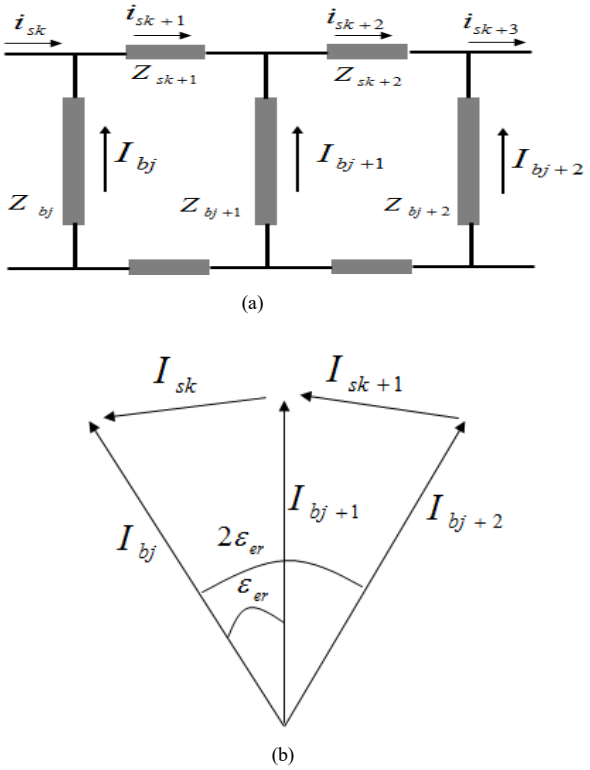

Fig. 3. Model of the rotor cage (only three bars are shown); (a) Equivalent model, (b) Rotor current phasor representation

The corresponding bar currents can be expressed as [20, 21]

$$I_{bj} = i_{sk+1} - i_{sk} = 2I_{sk} \sin\left(\frac{\varepsilon_{er}}{2}\right) \quad (1)$$

$$I_{bj+1} = i_{sk+2} - i_{sk+1} = 2I_{sk+1} \sin\left(\frac{\varepsilon_{er}}{2}\right) \quad (2)$$

$$I_{bj+2} = i_{sk+3} - i_{sk+2} = 2I_{sk+2} \sin\left(\frac{\varepsilon_{er}}{2}\right) \quad (3)$$

where ε_{er} is the time phase shift between currents in adjacent end ring segments I_{sk} and I_{sk+1}, and I_{bj} is the current in the bar j, which corresponds to the difference between currents in adjacent ring segments i_{sk} and i_{sk+1}.

III. FINITE ELEMENT ANALYSIS

This work is based on a finite element model of a SCIM. The induction machine is modelled with 2D Ansys Maxwell software. The dynamic and static analysis of the machine is performed for various rotor bar types for both healthy and

faulty conditions. The behaviour of the air-gap flux density is studied for different rotor bar types and operating conditions. The magnetic flux density distribution of the machine with rotor bar type 1 is presented in Fig. 4. In Fig. 5 the behaviour of the air-gap flux density for Type 1 rotor bar when three adjacent rotor bars per pole are broken is illustrated, the breakage of the rotor bars creates some distortion in the air-gap flux density. The air-gap flux density presented in Fig. 6 illustrates changes as rotor bars types are changed.

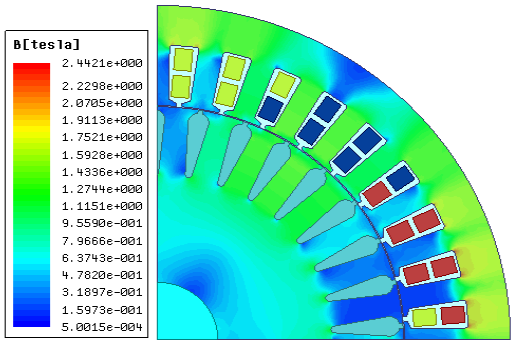

Fig. 4. Flux density distribution for machine with rotor bar Type 1 under healthy conditions.

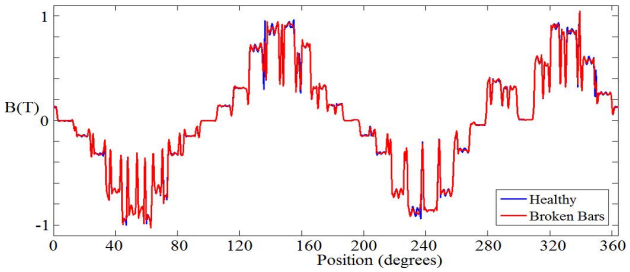

Fig. 5. Air-gap flux density for Type 1 rotor bar under healthy and faulty (3 adjacent broken rotor bars per pole) conditions.

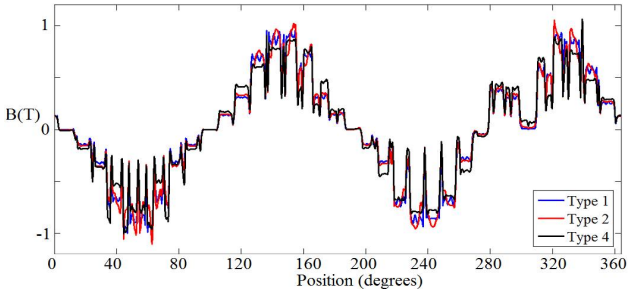

Fig. 6. Air-gap flux density for Types 1, 2 and 4 rotor bar under healthy conditions.

IV. ANALYSIS OF RESULTS

A. *Instantaneous torque*

Fig. 7 to Fig. 12 show the dynamic behavior of the motor from starting to steady state in relation to the toque. In Fig. 7 the starting behavior of different rotor bar shapes is illustrated, it is clear that changing the shape of the rotor bar will influence the starting performance of a motor because different rotor bar shapes will yield different rotor resistance. Rotor bar type 4 has smaller upper body cross-sectional area which results in increased rotor resistance hence a better starting torque compared to type 1 and 2. For all rotor bar types, the healthy machines seems to produce a smoother torque at starting as well as the steady state. As the motor is starting, the electromagnetic torque takes a negative direction because of very high inrush starting current and this results in voltage depression. This depression tends to significantly reduce the starting torque hence the torque is in a negative direction, but because of the skin effect phenomenon, the starting torque starts to take a positive turn as the starting current is reduced and the rotor bar current is evenly distributed throughout the bar [25, 27]. There is very high fluctuation in the starting torque for all faulty conditions compared to the healthy machine, this starting torque also seems to have a very high ripple content. Observing the starting torque between 0 ms to 20 ms, the torque ripple increases with increasing number of broken rotor bars.

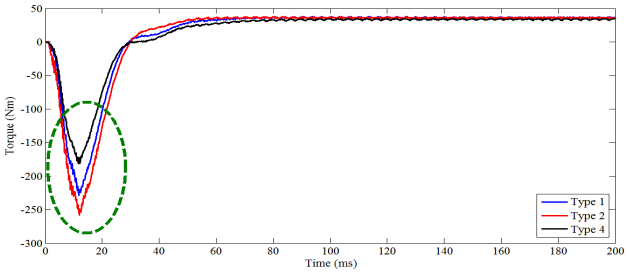

Fig. 7. Starting Torque for Type 1, 2 and 4 rotor bar under healthy conditions.

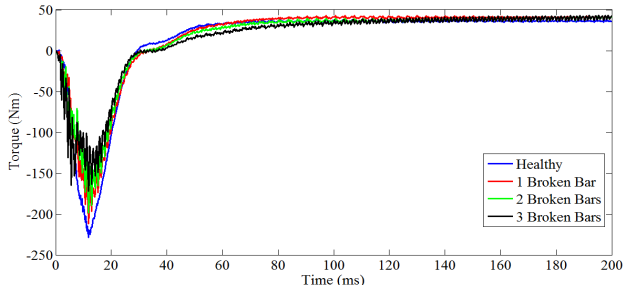

Fig. 8. Instantaneous Torque for Type 1 rotor bar under healthy and faulty (adjacent broken rotor bars) conditions.

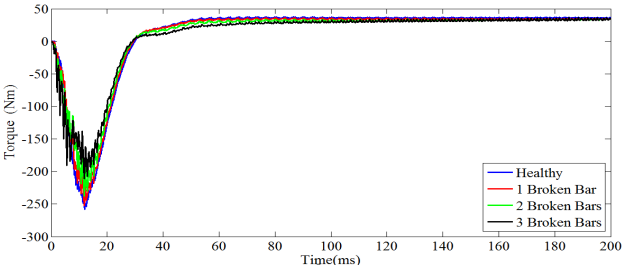

Fig. 9. Instantaneous Torque for Type 2 rotor bar under healthy and faulty (adjacent broken rotor bars) conditions.

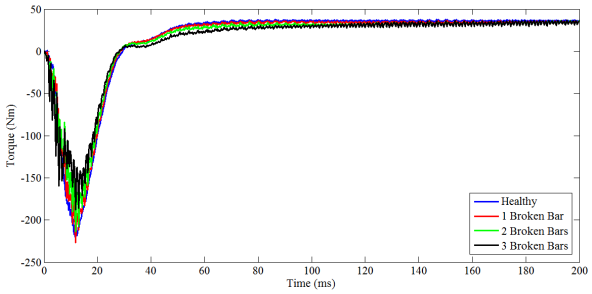

Fig. 10. Instantaneous Torque for Type 3 rotor bar under healthy and faulty (adjacent broken rotor bars) conditions.

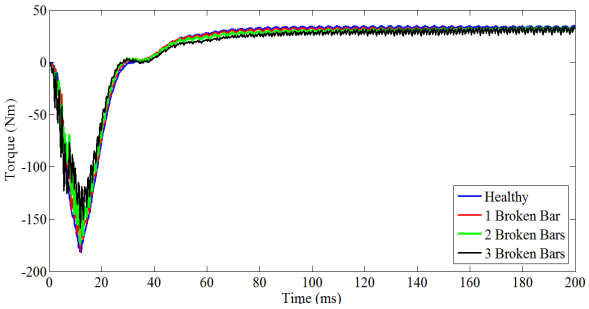

Fig. 11. Instantaneous Torque for Type 4 rotor bar under healthy and faulty (adjacent broken rotor bars) conditions.

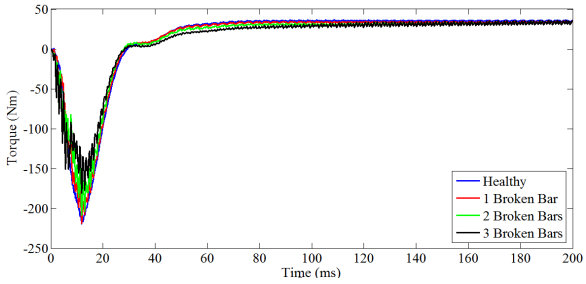

Fig. 12. Instantaneous Torque for Type 5 rotor bar under healthy and faulty (adjacent broken rotor bars) conditions.

B. *Steady-state torque*

Broken rotor bars have a significant impact on the steady-state average torque of three phase induction machines. A clearer representation of the steady state torque is presented in Fig. 13 to Fig. 17. The steady state torque for the for rotor bar type 1 in Fig. 13 shows a lower average value for a healthy machine compared to that of broken rotor bars. Although the average torque is lower, the healthy machine presents a much smoother torque compared to the faulty machine. When rotor bars break, harmonic components of the stator current are and this results in increased oscillation on the developed torque [15, 16]. Furthermore, the efficiency of rotor bar type 1 in Table VI is higher when the machine healthy than when rotor bars are broken. It can therefore be concluded that although the average torque of this rotor type under healthy conditions is lower, it still achieves a higher efficiency.

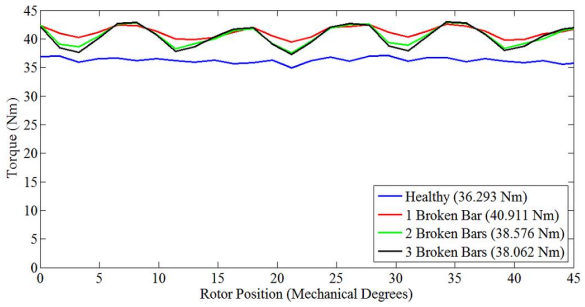

Fig. 13. Steady state Torque for Type 1 rotor bar under healthy and faulty (adjacent broken rotor bars) conditions.

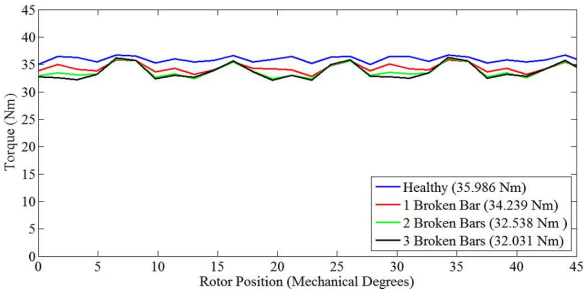

Fig. 14. Steady state Torque for Type 2 rotor bar under healthy and faulty (adjacent broken rotor bars) conditions.

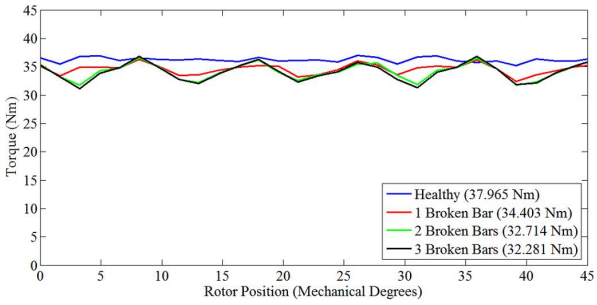

Fig. 15. Steady state Torque for Type 3 rotor bar under healthy and faulty (adjacent broken rotor bars) conditions.

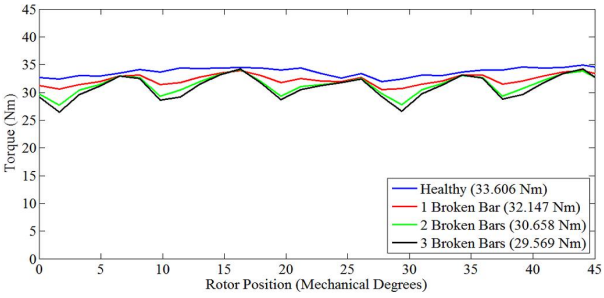

Fig. 16. Steady state Torque for Type 4 rotor bar under healthy and faulty (adjacent broken rotor bars) conditions.

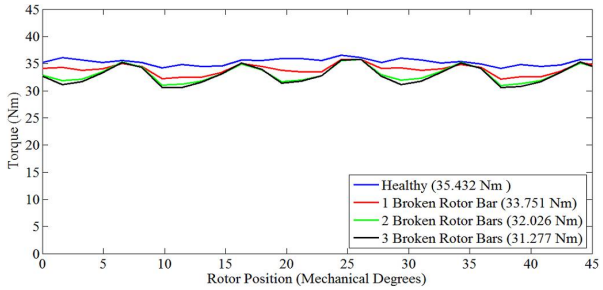

Fig. 17. Steady state Torque for Type 5 rotor bar under healthy and faulty (adjacent broken rotor bars) conditions.

Further results on the average torque and its ripple content are presented in Table IV and Table V. The rotor bar type that presents a better average torque under faulty is the rotor bar type 1 but there is a very high ripple content in this torque is very high. Under healthy conditions type 5 rotor bar , presents the list ripple content as compared to the rest of the bar types, this is also true for two broken rotor bars. From the results it is clear that increasing number of broken rotor bars leads to a significant increase ripple content in the torque and this results in a compromised performance of the machine. One other reason for increased ripple is redistribution of the current from broken bar/s to the adjacent ones creating an asymmetry in rotor bar currents, as reported in [29].

TABLE IV
AVERAGE TORQUE

Rotor Bar Type	Healthy (Nm)	1 Broken Bar (Nm)	2 Broken Bars (Nm)	3 Broken Bars (Nm)
Type 1	36.239	40.911	38.576	38.062
Type 2	35.986	34.239	32.538	32.031
Type 3	37.965	34.403	32.714	32.281
Type 4	33.606	32.147	30.658	29.569
Type 5	35.432	33.751	32.026	31.277

TABLE V
TORQUE RIPPLE

Rotor Bar Type	Healthy (%)	1 Broken Bar (%)	2 Broken Bars (%)	3 Broken Bars (%)
Type 1	10.903	10.829	21.182	32.028
Type 2	7.389	9.866	19.968	24.033
Type 3	10.518	12.670	22.140	28.444
Type 4	10.257	13.467	21.254	31.085
Type 5	7.124	10.622	18.897	29.594

C. *Efficiency and Power Factor*

One of the important aspects in energy saving is improvement of power factor and efficiency in induction machines, even a slightest improvement in efficiency can save a great deal of energy [19]. Rotor bar breakage as well as changes in rotor bar shapes causes the magnetic field to change, and this has an effect on the core losses which in turn affects the power factor and efficiency of the motor. Table VI presents the efficiency for different rotor bar types when the machine is healthy and when adjacent rotor bars are broken. For all the rotor bar types there is a slight or no change in the efficiency when only one rotor bar is broken. With the original rotor bar type, there is a noticeable decrease in efficiency under faulty conditions. The efficiency seems to increase for the rest of the rotor bar types when 1 and 2 rotor bar are broken, but as 3 bars break there is a slight decrease in efficiency. The rotor bar types that exhibits a better performance under faulty conditions as far as efficiency is concerned are rotor bar type 4 and 5.

As for the power factor presented in Table VII for various rotor bar types, the results prove a very slight but noticeable improvement in the overall power factor under healthy and faulty conditions. When the motor is healthy, rotor bar type 2 presents a better power factor compared to other rotor bar types. With adjacent broken rotor bars, rotor bars type 1 and 2 exhibit better power factor as compared to the rest of the rotor bar types. As the number of broken rotor bars increases from 2 to 3, the power factor increases with either 0.001 pu or 0.002 pu for all rotor bars except for type 5 with a significant increase of 0.025 pu.

TABLE VI
EFFICIENCY

Rotor Bar Type	Healthy	1 Broken Bar	2 Broken Bars	3 Broken Bars
	η (%)	η (%)	η (%)	η (%)
Type 1	76.189	72.511	74.917	74.732
Type 2	75.054	75.484	75.752	75.644
Type 3	76.923	77.331	77.534	77.424
Type 4	78.129	78.441	78.668	78.609
Type 5	77.003	79.668	79.752	77.556

TABLE VII
POWER FACTOR

Rotor Bar Type	Healthy	1 Broken Bar	2 Broken Bars	3 Broken Bars
	PF (pu)	PF (pu)	PF (pu)	PF (pu)
Type 1	0.882	0.927	0.897	0.899
Type 2	0.895	0.891	0.887	0.889
Type 3	0.874	0.869	0.867	0.868
Type 4	0.860	0.857	0.854	0.855
Type 5	0.873	0.844	0.842	0.867

V. CONCLUSION

In this paper, modeling and performance analysis of squirrel cage induction machine with broken rotor bars is carried out with use of Maxwell Ansys 2D Finite Element Method. The transient and steady-state behaviour of the machine is studied for both healthy and faulty conditions. The electromagnetic torque, torque ripple, air-gap flux density, efficiency and power factor under both conditions for different rotor bar types are studied. From the results it is clear that changes in the shape of a rotor bar has a significant impact in the overall performance of the machine. The steady-state torque remains stable under healthy conditions, whereas there is an intense fluctuation noticed in the presence of broken rotor bars. In general there is a small but noticeable decrease in efficiency and power factor when the number of broken rotor bars increases. The rotor bar type that seems to stand out in

performance under faulty conditions is rotor bar type 5, which is a rectangular bar type.

REFERENCES

[1] J Faiz and BM Ebrahimi, "Static eccentricity fault diagnosis in an accelerating no-load three-phase saturated squirrel cage induction motor", *Progress in electromagnetics research* B, 10, pp:35-54, 2008.

[2] LM Thusi, *Determining the optimal technique for early detection of broken rotor bars in medium voltage squirrel cage induction motors during operation*, Master of Science in Engineering, Johannesburg, Wits University, 2009

[3] S Salon, D Burow, M Debortoli and C Slavik, "Effects of slot closure and magnetic saturation on induction machine behavior", *IEEE Transactions on Magnetics,* 30 pp: 3697-3700, 2002

[4] EK Appiah, AA Jimoh, G M'boungui and JL Munda, "Effects of slot opening on the performance of six phase squirrel cage induction machine using finite element and field analysis", *AFRICON* 9-12 September 2013, pp: 1-5.

[5] S Bindu and VV Thomas, "Diagnoses of internal faults of three phase squirrel cage induction motor – A review". *Advances in Energy Conversion Technologies*, 23-25 January 2014, pp: 48-54.

[6] S Jelassi, R Romary and J Brudny, "Slot design for dynamic iron loss reduction in induction machines", *Progress in electromagnetics research B,* 14 May 2013:79-97.

[7] J Puranen, *Induction motor versus permanent magnet synchronous motor in motion control application: a comparative study,* Thesis for the degree of Doctor of Science (Technology), Finland, Lappeenranta University of Technology, 2006

[8] J Kappatou, C Gyftakis and A Safacas, "A study of the effects of stator slot wedges material on the behavior of induction machine", *ICEM 18th International Conference* 6-9 Sept. 2008:1-6.

[9] G Madescu, M Greconi and M Biriescu, "Effects of stator slot magnetic wedges on induction motor". *OPTIM 13th International Conference,* 24 -26 May 2012, 30, pp: 489-492.

[10] N Konstantinos, JC Kappatou, C Gyftakis and A Panagiotis, "Application of wedges for reduction of space and time-dependent harmonic content in squirrel cage induction machines", *Journal of Computational Engineering,* Volume (2013) 12 November 2013.

[11] SS Sivaraju and N Devarajan, "GA based optimal design of three phase squirrel cage induction motor for enhancing performance", *International Journal of Advanced Engineering Technologies,* Volume 2 October 2011, pp: 202-206.

[12] M Cunkas and R Akkaya, "Design optimization of induction motor by generic algorithm and comparison with existing motor", *Mathematical and Computational Applications,* Volume 11 2006:193-203.

[13] J Faiz, MBB Sharifian, A Keyhani and A Prpca, "Optimally designed induction motors with aluminum and copper squirrel cages", *Electric Machines and Power Systems,* Volume 28, 30 November 2010 pp: 1195-1207.

[14] VA Galindo, XM Lopez-Fedez, JAD Pinto and PA Coimbra, "Parametric study of rotor slot shape on a cage induction motor", *Studies in applied electromagnetic and mechanics,* 22, pp: 190-195, 2002

[15] J Faiz and BM Ebrahimi, "A new pattern for detecting broken rotor bars in induction machines during start-up", *IEEE Transactions on magnetics,* Volume 44, December 2008, pp: 4673-4683.

[16] Y Xie, C Gu and W Cao, "Study of broken bars in three-phase squirrel cage induction motors at standstill". *International Transactions on Electrical Energy Systems,* 2013; 23, pp: 1124–1138.

[17] A Ceban, R Romary and R Pusca, "A new pattern for detecting broken rotor bars in induction machines during start-up". *IEEE Transactions on Industrial Electronics,* Volume 44, May 2012, 59(5): 2082-2093.

[18] Y Xie, "Investigation of broken rotor bar faults in three-phase squirrel-cage induction motors, Finite Element Analysis" - *From Biomedical Applications to Industrial Developments,* Dr. David Moratal (Ed.), ISBN: 978-953-51-0474-2. Pp: 477-496.

[19] YS Kim, "Effects of Rotor Bar Shape for Squirrel Cage Induction Motor in Transient State Using Moving Band Technique". *IEEE Trans. on Applied Superconductivity,* Volume 24, Issue: 3, June 2014.

[20] I Boldea and L Tutelea, *Electrical Machines: Steady State, Transients, and Design with Matlab*, CRC Press, Boca Raton, Florida, USA, 2009.

[21] I Boldea and SA Nasar, *The Induction Machine Handbook*, CRC, Boca Raton, Florida, USA, 2001.

[22] TA Lipo, *Introduction to AC Machine Design*, Madison, WI: University of Wisconsin Press, 1996.

[23] AK Wallace and A Wright, "Novel Simulation of Cage Windings Based on Mesh Circuit Model", *IEEE Transactions on Power Application Systems,* Vo. PAS-93, pp. 377-382, Jan/Feb 1974.

[24] AR Monoz and TA Lipo, "Complex Vector Model of Squirrel-Cage Induction Machine Including Instantaneous Rotor Bar Currents", *IEEE Trans. on Power Application Systems,* Vol. PAS-93, pp. 377-382, Jan/Feb 1974.

[25] R Hung & HW Dommel, Synchronous Machine Models for Simulation of Induction Motor Transient, *IEEE transactions on Power Application Systems,* Vo. 11, pp: 833-838, May 1996.

[26] HJ Coelingh, PC Breedveld & J van Dijk, Modeling of Three Phase Induction Machine with Rotor Skin-Effect, *2nd IMACS International Multi-conference CESA'98, IEEE,* PP. 535-540, 1998.

[27] A Dey, A Tripahti, B Singh, B Dwivwdi & D Chadra, An Improved Model of a Three Phase Induction Motor Incorporating the Parameter Variations. *Electrical Power Quality and Utilization, Journal* Vo. XIV, pp: 73-78, 2008.

[28] R. Campeanu, M. Cernat „Two Speed Single Phase Induction Motor with Electronically Controlled Capacitor," Advances in Electrical and Computer Engineering, Suceava, Romania, Year: 2014, Volume: 14, Number: 3 (August 2014), Page(s): 137 – 140, DOI:10.4316/AECE.2014.03018

[29] G. Badescu, M Biriescu, LN Tutelea, M Mot, M. Svoboda and I. Boldea, "Experimental Investigation of Rotor Currents Distribution in Three Phase Induction Motors with Symmetrical Squirrel Cage at Standstill", 2016 XXII *International Conference on Electrical Machines* (ICEM), pp 338-343